NJC

Accepted Manuscript

This is an *Accepted Manuscript*, which has been through the Royal Society of Chemistry peer review process and has been accepted for publication.

Accepted Manuscripts are published online shortly after acceptance, before technical editing, formatting and proof reading. Using this free service, authors can make their results available to the community, in citable form, before we publish the edited article. We will replace this *Accepted Manuscript* with the edited and formatted *Advance Article* as soon as it is available.

You can find more information about *Accepted Manuscripts* in the Information for Authors.

Please note that technical editing may introduce minor changes to the text and/or graphics, which may alter content. The journal's standard Terms & Conditions and the Ethical guidelines still apply. In no event shall the Royal Society of Chemistry be held responsible for any errors or omissions in this *Accepted Manuscript* or any consequences arising from the use of any information it contains.

ROYAL SOCIETY OF CHEMISTRY

www.rsc.org/njc

Photocatalytic Properties of Bi/BiOCl Heterojunctions Synthesized by In Situ Reduction Method

Jiajia Hu[1], Guangqing Xu[1*], Jinwen Wang[1], Jun Lv[1], Xinyi Zhang[1], Zhixiang Zheng[1], Ting Xie[3], Yucheng Wu[1, 2*]

1 Laboratory of Functional Nanomaterials and Devices, School of Materials Science and Engineering, Hefei University of Technology, Hefei 230009, China

2 Anhui Provincial Key Laboratory of Advanced Functional Materials and Devices, Hefei University of Technology, Hefei 230009, China.

3 Institute of Tribology, Hefei University of Technology, Hefei 230009, China.

Abstract: Bi nanoparticles are grown on BiOCl nanosheets via an in situ chemical reduction in KBH_4 aqueous solution. Bi/BiOCl nanosheets with different content of Bi nanoparticles can be achieved by changing the concentration of KBH_4 solution. The structure, morphology, elemental composition and optical absorption performance are characterized by using X-ray diffraction diffractometer, scanning electron microscope, high resolution transmission electron microscope, X-ray photoelectron spectroscope and UV-Vis diffuse reflection spectroscope. The photocatalytic activities of the as-prepared photocatalysts are tested by the degradation of methyl orange under both UV light and visible light irradiation. Bi nanoparticles modified on BiOCl nanosheets not only enhance the photocatalytic activity under UV light irradiation, but also achieve visible light photocatalytic activity. The mechanisms of Bi nanoparticles modification are discussed in the whole photocatalytic processes, such as optical absorption, chargers transfer and surface reactions.

Key words: Bi nanoparticles; BiOCl nanosheets; Heterojunctions; In situ reduction; Photocatalysis

1 Introduction

Semiconductor photocatalysts have attracted a great deal of attention due to their application in the field of pollutants degradation in the waste water and air [1, 2]. Photocatalysis has been considered as the most potential resolution to solve the pollution problems in the last few years. TiO_2 is one of the earliest and most widely researched semiconductors for environment protection owing to its outstanding photocatalytic efficiency, nontoxicity and high stability [3].

In recent years, as alternatives to TiO_2, Bi-based photocatalysts, such as $BiVO_4$[4, 5], Bi_2O_3[6, 7], Bi_2WO_6[8, 9], BiOCl [10, 11], have been widely studied in photocatalytic applications. Among these

* Corresponding author: Tel.: +86 551 62901372
Email address: gqxu1979@hfut.edu.cn (Guangqing Xu)
ycwu@hfut.edu.cn (Yucheng Wu)

photocatalysts, bismuth oxychloride (BiOCl) has been paid much attention because of its unique optical, electrical and catalytic properties. BiOCl has a layer structure that formed by alternately arranged double Cl atoms layers and [Bi2O2] layers along the c-axis, which can also be expressed as [Cl-Bi-O-Bi-Cl] [12]. This layer structure has enough space to polarize the corresponding atoms and atomic orbital and the induced dipole moment could separate the photoinduced electrons and holes effectively, so that the recombination rate of photoinduced electrons and holes is decreased.

However, the limited optical absorption and recombination of photoinduced electrons and holes also restrict the development of BiOCl. Therefore, noble metal modification was raised and studied by scientists, such as Pt[13], Au[14], Ag[15] and so on. The metal nanoparticles can form Schottky barrier at the interface of semiconductors, which serves as an electron trap, and improves the separation of electron-hole pairs. Therefore the photocatalytic performance can be effectively promoted. Edwards' group studied different metals deposited on BiOCl and found that different deposited metal presented different improvement of photocatalytic properties of BiOCl[16].

Bismuth (Bi) is a semimetal with a very small band gap possessing highly anisotropic Fermi surface, low carrier densities, small carrier effective masses, and long carrier mean free path [17]. When Bi nanoparticles are smaller than a few tens of nanometers, a semimetal to semiconductor transition takes place [18]. Similar to Ag nanoparticles, Bi nanoparticles have been found to exhibit plasmonic properties [19]. Collective excitation of free electrons in conduction band of semimetal Bi gives rise to the surface plasmon resonance (SPR) phenomenon, which results in a strong resonant optical absorption and many applications, such as sensors, fluorescence, surface-enhanced spectroscopy and photocatalysis [20].

Compared to general noble metal modification, Bi nanoparticles modified BiOCl synthesized by in situ reduction method is much easier to prepare and the cost is more economical [21]. Because Bi nanoparticles are generated from BiOCl matrix by in situ reduction, the combination of Bi and BiOCl is much better than that prepared by common depositions and the lattice matching in the interface is also better. A better lattice matching is beneficial to the transfer of charges, thus enhance the photocatalytic activity of the semiconductor.

Here, Bi nanoparticles modified BiOCl (Bi/BiOCl) nanosheets were prepared by in situ chemical reduction in KBH_4 solution at room temperature, which results in uniform distribution of Bi nanoparticles on the BiOCl nanosheets, and the amount of Bi nanoparticles is controllable.

2 **Experimental**

2.1 Synthesis

Bismuth nitrate pentahydrate ($Bi(NO_3)_3 \cdot 5H_2O$), sodium chloride (NaCl), KBH_4, ethylene glycol (EG) and terephthalic acid were purchased from Sinopharm Chemical Reagent Co., Ltd. (Shanghai, China). All reagents were analytical grade and used as received without further purification.

BiOCl nanosheets were synthesized via solvothermal method. In a typical procedure, 0.97 g $Bi(NO_3)_3 \cdot 5H_2O$ (2 mmol) was dissolved in 25 mL EG, and 0.117 g NaCl (2 mmol) was dissolved in 25 mL distilled water. The NaCl solution was added dropwise into $Bi(NO_3)_3$ solution under stirring condition. After being stirred for 30 min, the mixed solution was transferred to a teflon-lined stainless autoclave. The solvothermal synthesis was conducted at 150℃ for 10 h in an electric oven. The resulting precipitate was washed with ethanol and deionized water several times. Finally, the white powdered BiOCl was obtained by drying the precipitate at room temperature in air.

Bi nanoparticles deposition was performed via an in situ reduction in KBH_4 solution. 0.5 g BiOCl powder was added to 40 mL KBH_4 solution with different concentrations ranging from 5 to 100 mmol L^{-1} respectively, and reacted for 10 min under stirring. The resulting products were washed with ethanol and deionized water several times to remove the retained reaction solution. The final Bi/BiOCl nanosheets were obtained by drying the precipitates at room temperature in air. The Bi/BiOCl nanosheets prepared with different KBH_4 solution are defined as Bi/BiOCl-5, Bi/BiOCl-12.5, Bi/BiOCl-25, Bi/BiOCl-50 and Bi/BiOCl-100 nanosheets, respectively.

2.2 **Characterization**

X-ray diffraction (XRD) patterns, performed on a D/MAX2500V diffractometer using Cu Kα radiation at a scan rate of 2°/min ranging from 10° to 70°, were used to confirm the phase structure of the samples. The morphologies and microstructures of the products were investigated by field emission scanning electron microscope (FESEM, Hitachi SU8020) and high resolution transmission electron microscope (HRTEM, JEM-2100F). The TEM samples were prepared by grinding and dispersing the powder in ethyl alcohol with ultrasonication for 20 min. Carbon-coated copper grids were used as sample holders. X-Ray photoelectron spectroscopy (XPS) measurements were performed on an ESCALAB 250 photoelectron spectrometer using a monochromatic Al Ka X-ray beam (1486.60 eV). Diffuse reflectance spectroscopy (UV-Vis) DRS measurement was carried at room temperature on a CARY 5000 spectrometer (Agilent，USA) by using $BaSO_4$ as reference.

Concentration of HO· in the solution during photocatalytic process was detected by terephthalic acid oxidation method [22]. Terephthalic acid can react with HO· and the product of dihydroxy

terephthalic acid shows excellent photoluminescence properties with emission peak wavelength at around 420 nm when excited by UV light at 315 nm. Photoluminescence (PL) spectra were measured using a UV3600 spectrometer (Shimadzu, Japan) to monitor the HO· concentrations during photocatalytic process.

2.3 Photocatalysis

Methyl Orange (MO) solution was used to evaluate the photocatalytic activity of the BiOCl and Bi/BiOCl nanosheets. 0.01 g photocatalyst powders were placed in 10 mL MO solution with the concentration of 20 $mg \cdot L^{-1}$, and vigorously stirred for 30 min to achieve the adsorption/desorption equilibrium in the dark. A 300 W high-pressure mercury lamp (with a maximum emission wavelength at 364 nm) was used as UV light source and a 250 W metal halide lamp (with UV light filters removing the light source shorter than 420 nm) was used as visible light source. The photocatalytic reactions were performed on a XPA-7 photochemical reactor (Nanjing Xujiang Machine-electronic Company, China). The distance between the solution and the lamp was kept at 10 cm. Every 2 min (UV light irradiation) or 30 min (visible light irradiation) 5 mL solution was collected from the suspension and centrifuged, then the upper clear solution was measured by a UV1800 spectrometer (Shimadzu, Japan) to record the concentration of MO after being photodegraded.

3 Results and discussion

Bi nanoparticles modified BiOCl nanosheets are prepared by in situ chemical reduction of BiOCl nanosheets in KBH_4 solution at room temperature. The structure, morphology, elemental composition and optical absorption performance are characterized and the photocatalytic activities of the as-prepared photocatalysts are tested by the degradation of methyl orange under both UV light and visible light irradiation.

3.1 Structure and morphology

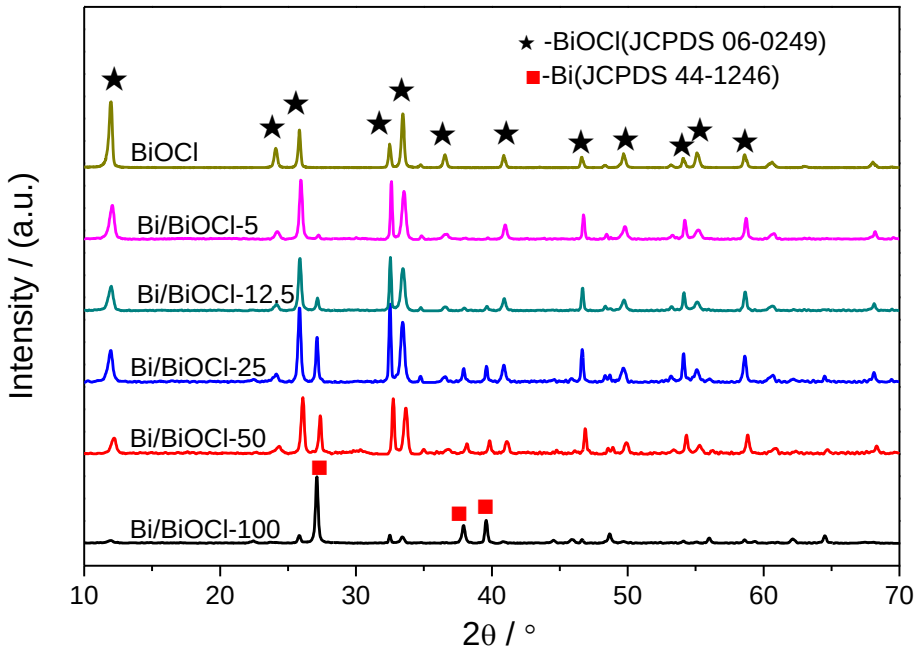

Fig.1 XRD patterns of BiOCl nanosheets and Bi/BiOCl nanosheets prepared with KBH_4 concentrations ranging from 5 to 100 mmol L^{-1}.

Fig.1 shows the XRD patterns of as-synthesized BiOCl nanosheets and Bi/BiOCl nanosheets prepared in KBH_4 solution with different concentrations of 5, 12.5, 25, 50 and 100 mmol L^{-1}, respectively. As being shown in Fig.1, all the diffraction peaks in the XRD pattern of pure BiOCl nanosheets are perfectly in good agreement with the tetragonal phase of BiOCl (JCPDS File No.06-0249) and no impurities can be detected, demonstrating that the product is BiOCl of high purity and well crystallized. In addition, no diffraction peaks of metallic Bi can be observed in BiOCl nanosheets. However, XRD patterns of Bi/BiOCl nanosheets after being reduced by KBH_4 are different to that of BiOCl nanosheets. Some new diffraction peaks can be observed in addition to the diffraction peaks appeared in BiOCl nanosheets. The newly appeared diffraction peaks with 2θ value of 27.1 º, 37.9 ºand 39.6 ºare corresponding to the (012), (104) and (110) lattice planes of metallic Bi (JCPDS File No. 44-1246) respectively, indicating that part of BiOCl was reduced to metallic Bi, and Bi/BiOCl nanosheets were achieved. From the comparison of Bi/BiOCl nanosheets prepared with different KBH_4 concentrations, the peak intensities of BiOCl become weaker and that of metallic Bi go stronger when increasing the concentration of KBH_4 solution, indicating that the content of Bi nanoparticles can be adjusted via changing the concentration of reductant.

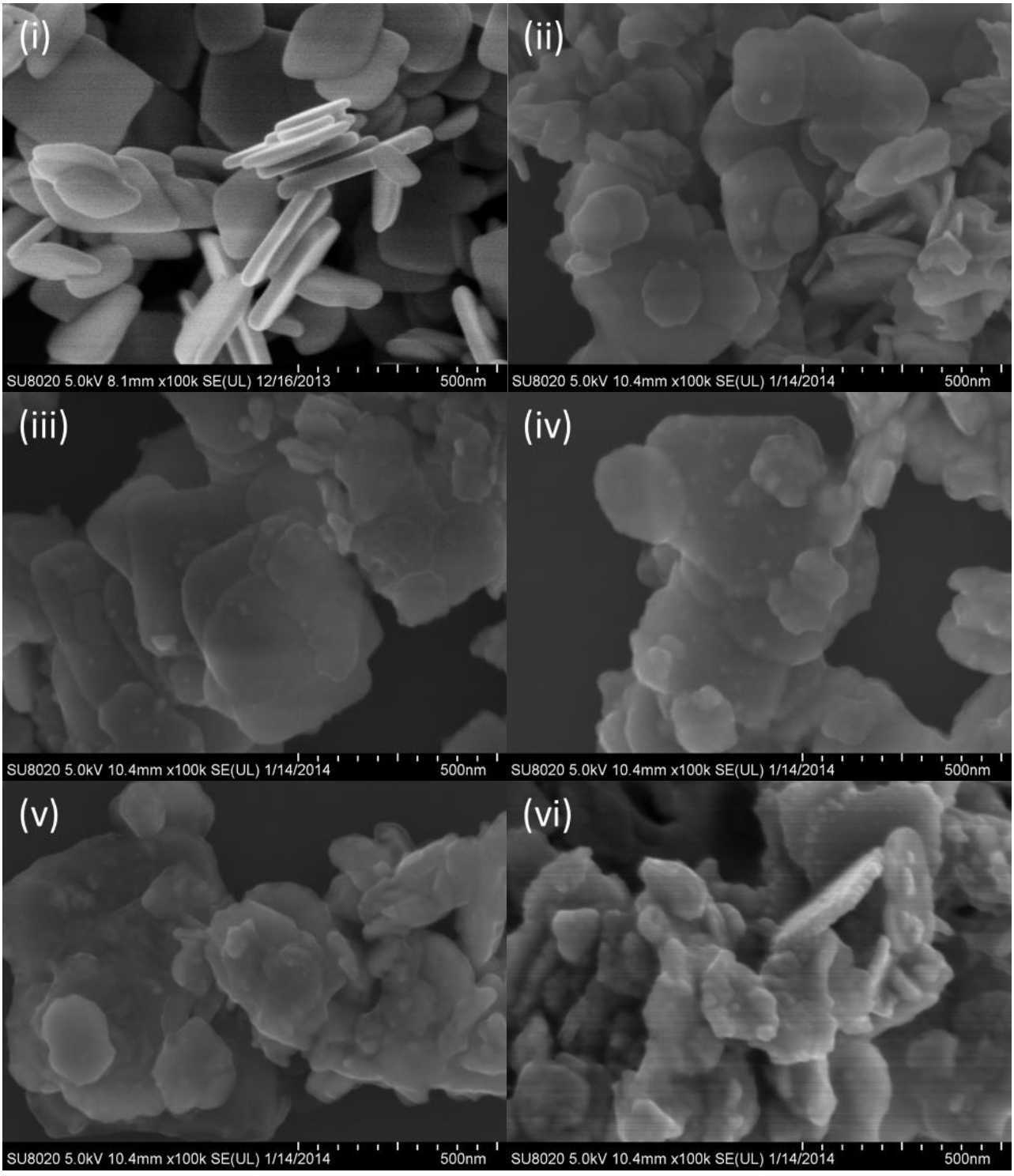

Fig.2 SEM images of BiOCl (i) and Bi/BiOCl with different concentration of KBH_4 solution, (ii) 5 mmol L^{-1}, (iii) 12.5 mmol L^{-1}, (iv) 25 mmol L^{-1}; (v) 50 mmol L^{-1}, (vi) 100 mmol L^{-1}.

Fig.2 shows the SEM morphologies of as-prepared BiOCl nanosheets and Bi/BiOCl nanosheets prepared with different KBH_4 concentrations. Fig.2(i) is the morphology of BiOCl nanosheets without further treatment. The pure BiOCl is mainly composed of quite uniform sheets with width of 300~500 nm and thickness of approximately 30~50 nm, and the surface of the BiOCl nanosheets is

smooth without any impurities. Fig.2(ii)~(vi) are the morphologies of Bi/BiOCl nanosheets prepared with different KBH_4 concentrations of 5 (ii), 12.5 (iii), 25 (iv), 50 (v) and 100 mmol L^{-1} (vi) respectively. When BiOCl nanosheets were treated with KBH_4, nanoparticles with size from 5 to 20 nm appeared on the surface of BiOCl nanosheets, and the shape of BiOCl nanosheets became irregular to some extent. These are Bi nanoparticles reduced in situ from BiOCl nanosheets. From the comparison of Bi/BiOCl nanosheets with different KBH_4 concentrations, the quantity of nanoparticles increases gradually and the shape of BiOCl substrate is getting more and more irregular with an increase of KBH_4 concentrations.

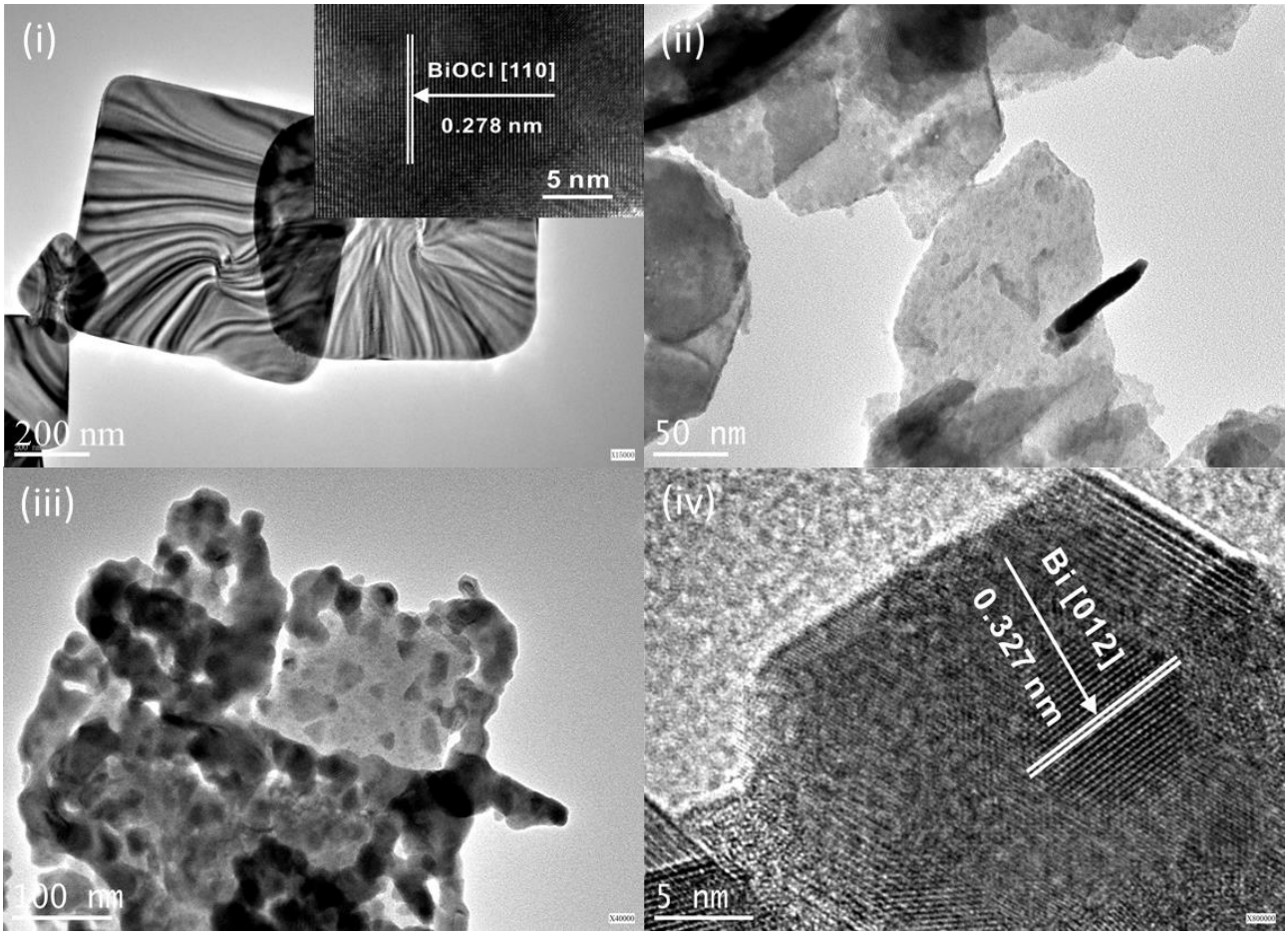

Fig.3 TEM and HRTEM morphologies of BiOCl nanosheets and Bi/BiOCl nanosheets prepared in different KBH_4 solution , (i) BiOCl nanosheets, inset is the HRTEM view of BiOCl nanosheets, (ii) Bi/BiOCl-25, (iii) Bi/BiOCl-100, (iv) HRTEM of Bi/BiOCl-25.

To further investigate the morphologies, the as-synthesized BiOCl nanosheets, Bi/BiOCl-25 and Bi/BiOCl-100 were also characterized by high resolution transmission electron microscopy, and the results are shown in Fig.3. Fig.3 (i) is the TEM morphology of as-synthesized BiOCl nanosheets, from which the smooth surface of the nanosheets can be observed. The HRTEM morphology of BiOCl is shown in the top right inset. The lattice space is measured to be 0.278 nm, which

corresponds to the (110) lattice plane of BiOCl. These BiOCl nanosheets with single crystalline structure have been reported many times [23]. Fig.3 (ii) and (iii) show the Bi/BiOCl-25 and Bi/BiOCl-100 nanosheets respectively. The visual field is composed of some nanosheets with a large amount of nanoparticles of approximately 5~20 nm bestrewed on them. When KBH_4 concentration is 25 mmol L^{-1}, the nanoparticles are evenly distributed on BiOCl nanosheets without any agglomerations and the nanosheets are intact without visible damage. However, when KBH_4 concentration is 100 mmol L^{-1}, the nanosheets suffer serious damage compared to that with low concentration, and the nanoparticles on Bi/BiOCl-100 nanosheets are much bigger than that of Bi/BiOCl-25 nanosheets. Fig.3(iv) is the HRTEM morphology of Bi/BiOCl-25 nanosheets. The nanoparticles exhibit good crystalline and clear lattice fringes. The interplanar spacing are 0.327 nm, which corresponds to the (012) lattice plane of metallic Bi (JCPDS File No. 44-1246). Combined with the results of XRD pattern in Fig.1, these nanoparticles can be confirmed to be metallic Bi reduced from BiOCl nanosheets.

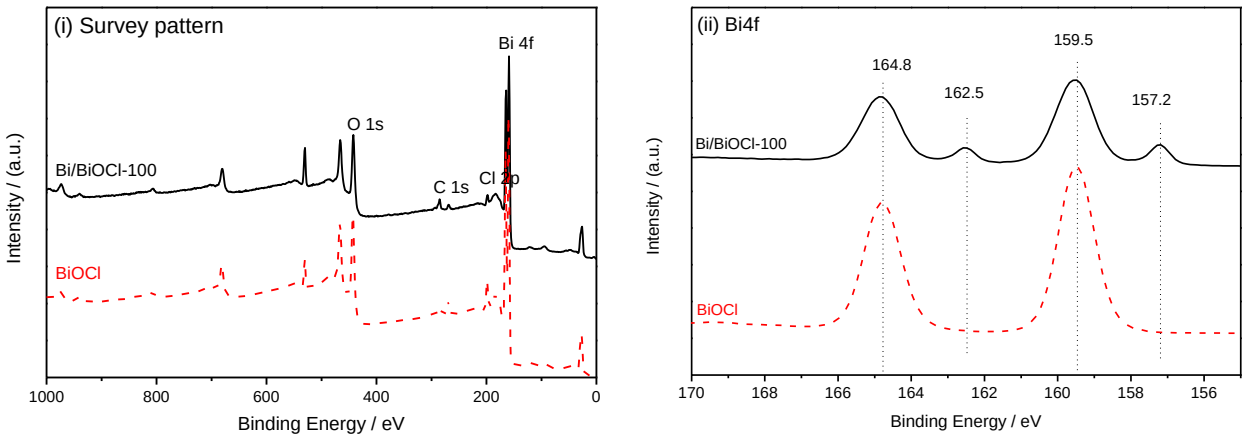

Fig.4 XPS patterns of BiOCl and Bi/BiOCl-100 nanosheets. (i) Survey pattern, (ii) high resolution pattern of Bi 4f electrons.

The XPS spectra are measured to confirm the elemental composition of BiOCl and Bi/BiOCl-100 nanosheets and shown in Fig.4. Fig.4 (i) shows the XPS survey spectra of the two samples. The main composition of the samples can be obtained to be Bi, O and Cl with the binding energy peaks at 163 eV (Bi 4f), 442 eV (O 1s) and 285 eV (Cl 1s) respectively. Peak of C1s at 284.7 eV, existing in both samples, is originated from the testing process of XPS. The high-resolution XPS spectra of two samples in the regions of Bi 4f are shown in Fig.4 (ii). Two peaks with binding energy at 159.5 eV and 164.4 eV can be observed in spectrum of BiOCl nanosheets, which can be ascribed to Bi^{3+} 4f 7/2 and Bi^{3+} 4f 5/2 binding energies, respectively. The result shows that only triple charged Bi ions exist in the sample. However, in the spectrum of Bi/BiOCl-100 nanosheets, apart from the two peaks discussed above, there are two peaks at 162.5 eV and 157.2 eV with low intensity, which can be

ascribed to the metallic Bi. Therefore, the sample after being reduced not only contains BiOCl, but also metallic Bi reduced from BiOCl nanosheets. The results of XRD, SEM, HRTEM and XPS prove that the Bi/BiOCl composite photocatalysts are successfully synthesized.

3.2 Optical absorption performance

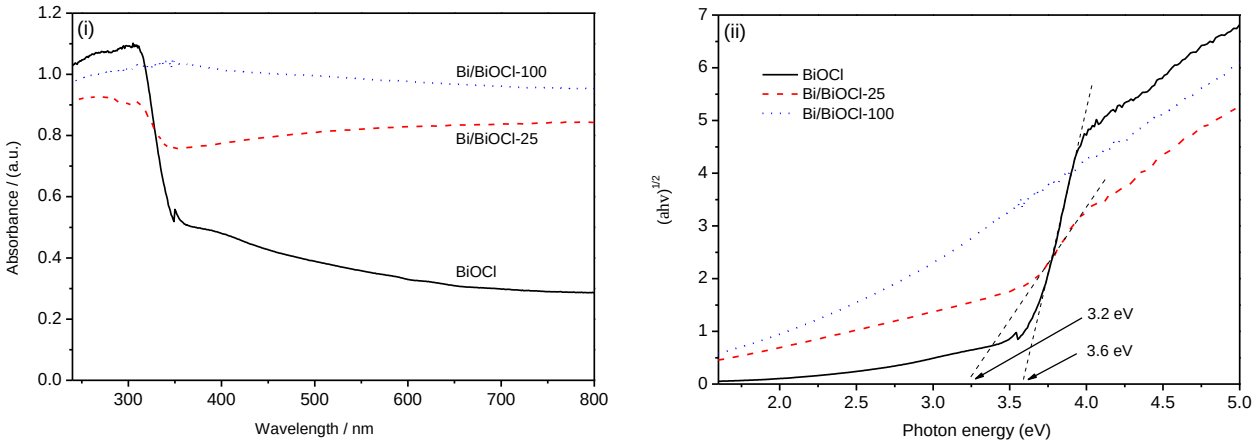

Fig.5 UV-Vis absorption spectra (i) and transformed Kubelka-Munk function vs. photon energy (ii) of BiOCl, Bi/BiOCl-25 and Bi/BiOCl-100 nanosheets.

UV-Vis diffuse reflectance spectrum (DRS) is an effective method to characterize the optical property of semiconductor samples. Fig.5 shows the UV-Vis absorption spectra and the transformed Kubelka-Munk function vs. photon energy of BiOCl, Bi/BiOCl-25 and Bi/BiOCl-100 nanosheets. From Fig.5 (i), only a strong absorption intensity is exhibited in the UV region for BiOCl nanosheets with an absorption edge at approximately 350 nm, indicating that BiOCl is optical inert in the visible region. A continuous absorption band in the visible region from 350 to 800 nm can be observed when modified with Bi nanoparticles, which is in accordance with the black color of Bi/BiOCl samples. The visible light absorption of Bi/BiOCl nanosheets can be ascribed to the indirect band gap transition and SPR effect of semiconductor Bi nanoparticles. The absorption edge of Bi/BiOCl-25 nanosheets is similar with that of as-prepared BiOCl nanosheets. However, no absorbance peaks and absorbance limits of Bi/BiOCl-100 nanosheets can be observed due to the high concentration of KBH_4, in which large quantity of BiOCl has been converted to metallic Bi, indicating low photocatalytic activities of Bi/BiOCl-100 nanosheets.

Through the spectrum, the band gap of a semiconductor can be simply calculated by the following equation: $\alpha h\upsilon = A(h\upsilon - Eg)^{n/2}$, where α, υ, A, and Eg are the absorption coefficient, light frequency, proportionality constant and band gap energy, respectively[24]. Among them, n depends on the characteristics of the transition in a semiconductor (n=1 for direct transition or n = 4 for indirect transition). Here, the value of n is 4 because BiOCl is an indirect semiconductor [25]. Therefore, the

band gap energies of the BiOCl samples could be estimated from a plot of $(\alpha h\upsilon)^{1/2}$ versus the photon energy ($h\upsilon$) as shown in Fig.5(ii). The intercepts of the tangent to the x-axis will give a good approximation of the band gap energies for the BiOCl and Bi/BiOCl samples. The estimated band gap energy of the BiOCl nanosheets is approximately 3.6 eV, while the value of Bi/BiOCl-25 nanosheets is approximately 3.2 eV, which is narrower than that of BiOCl nanosheets due to the introduction of Bi into the Bi/BiOCl nanosheets.

3.3 Photocatalytic activity

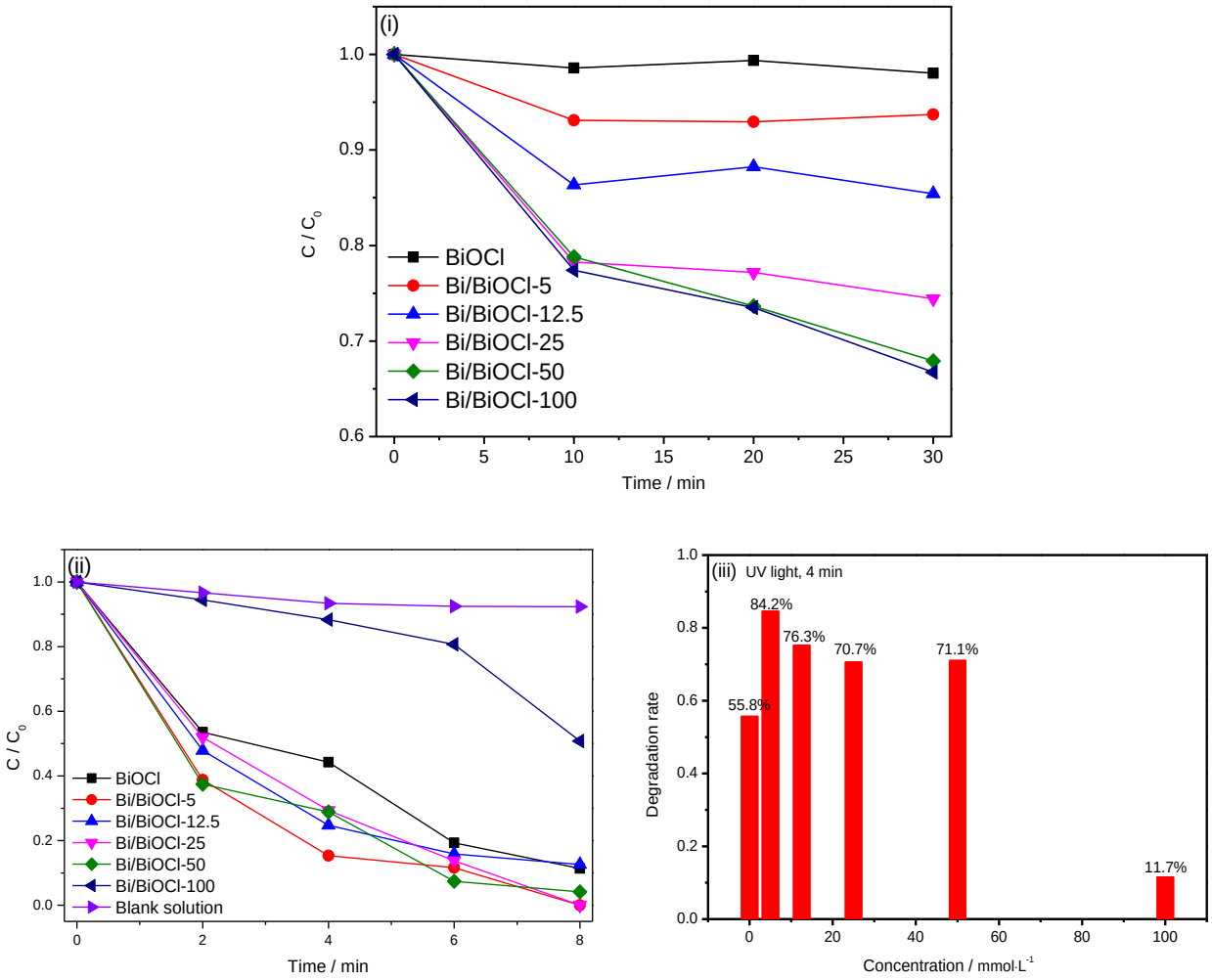

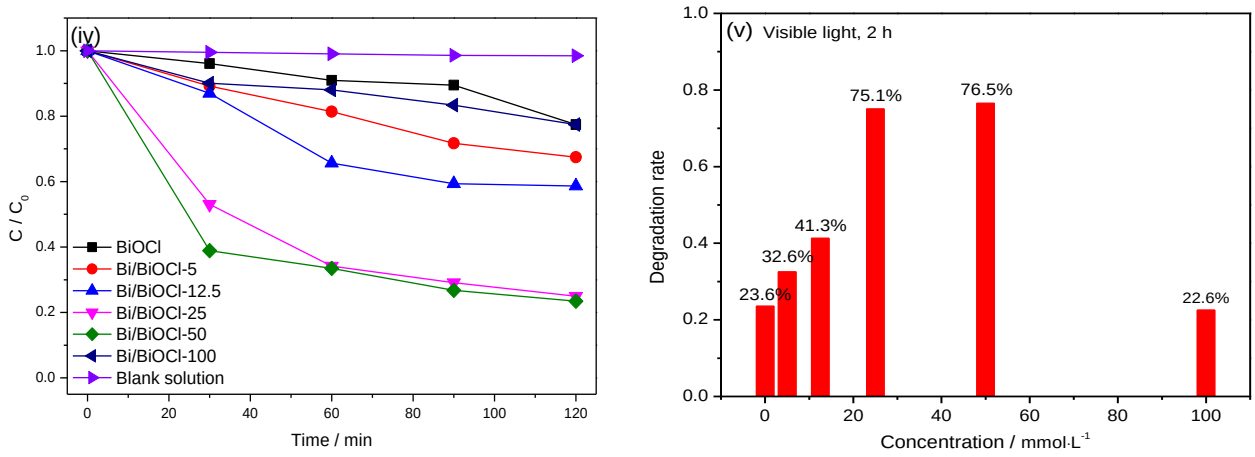

Fig.6 Adsorption (i) and Photocatalytic performances of BiOCl nanosheets and Bi/BiOCl nanosheets prepared in KBH_4 solution with different concentrations under UV (ii, iii) and visible (iv, v) light irradiation.

The photocatalytic activities of BiOCl and Bi/BiOCl samples were measured by the degradation of MO solution under UV light and visible light irradiation respectively. Before degradation, the adsorption/desorption equilibrium was achieved by stirring the solution vigorously for 30 min in the dark at room temperature. The characteristic absorption peak of MO at 464 nm was used to detect the photocatalytic degradation process.

Fig.6 shows the adsorption (i) and photocatalytic properties of BiOCl and Bi/BiOCl nanosheets under UV light (ii, iii) and visible light (iv, v) irradiation respectively. Fig.6 (i) shows the adsorption properties of BiOCl and Bi/BiOCl nanosheets prepared with different KBH_4 concentrations. BiOCl nanosheets with smooth surface show poor adsorption performance and the adsorption rate is only 2% after 30 min. The adsorption performances of Bi/BiOCl nanosheets are better than that of BiOCl nanosheets and increase with the concentration of KBH_4 solutions, such as 6.3% for Bi/BiOCl-5, 14.6% for Bi/BiOCl-12.5, 25.6% for Bi/BiOCl-25, 32.1% for Bi/BiOCl-50 and 33.3% for Bi/BiOCl-100. The rough surfaces of Bi/BiOCl nanosheets formed in the reduction process possess high adsorption performance than the smooth surface of BiOCl nanosheets. The surface areas of BiOCl and Bi/BiOCl nanosheets are tested, which are 11.801 and 18.829 m^2/g respectively. The increase of the surface area after being reduced results in the enhancement of adsorption performance of BiOCl nanosheets.

Fig.6(ii) shows the ratio of MO concentration C at appointed time interval and initial MO concentration C_0 (C/C_0) versus the degradation time under UV light irradiation when being degraded with different samples. MO was photodegraded directly by UV light a little with degradation rate of 7.67% in 8 min. BiOCl nanosheets show excellent photocatalytic activities under UV light irradiation, which has been confirmed by many researchers[26, 27]. Here, when treated with BiOCl nanosheets, the

MO concentration decreases gradually with the degradation time. And the as-synthesized BiOCl nanosheets can achieve 90% degradation rate only in 8 min. Bi nanoparticles on BiOCl nanosheets can enhance the photocatalytic activities, and most Bi/BiOCl nanosheets can achieve the degradation rate as high as 90% or more after 8 min irradiation, except for Bi/BiOCl-100 nanosheets.

In consideration that as-prepared BiOCl nanosheets have good photocatalytic performance, which can achieve degradation ratio of 90% in 8 min. For convenient comparison, the degradation rates of all samples irradiated under UV light for 4 min are extracted to obtain the effects of Bi nanoparticles modification. The degradation rates of BiOCl and Bi/BiOCl nanosheets prepared with different KBH_4 concentrations after being irradiated in UV light for 4 min are shown in Fig.6 (iii). 0 in horizontal axis means BiOCl nanosheets without further reduction. In 4 min, BiOCl nanosheets achieve degradation rate of 55.8%. Bi nanoparticles can enhance the degradation rate in most cases except for Bi/BiOCl-100 nanosheets, which is only 11.7% when irradiated in UV light for 4 min. The degradation rate achieves the maximum of 86.2% when KBH_4 concentration is 25 mmol L^{-1}.

Fig.6 (iv) is the ratio of MO concentration at appointed time interval and initial MO concentration C_0 (C/C_0) versus the degradation time under visible light irradiation when being degraded with different samples. MO is very stable under visible light illumination with only photodegradation rate of 1.54% in 2 h. BiOCl nanosheets show poor visible light photocatalytic performance, and the degradation rate is only 20% after being irradiated for 2 h. After being reduced by KBH_4 solution, the photocatalytic activities of Bi/BiOCl nanosheets in visible light are improved, that is the photocatalytic properties of Bi/BiOCl nanosheets are better than that of BiOCl nanosheets, especially the Bi/BiOCl nanosheets prepared in 25 and 50 mmol L^{-1} KBH_4 solutions.

Fig.6 (v) compares the degradation rates of BiOCl and Bi/BiOCl nanosheets after being irradiated under visible light for 2 h. After being irradiated for 2 h, the degradation rate of blank BiOCl is only 23.6%, and Bi nanoparticles modification increases the degradation rate under visible light obviously. In a whole, the photocatalytic properties of Bi/BiOCl increase gradually with the reductant concentration changing from 0 to 50 mmol L^{-1}, and the obtained samples reduced in 25 and 50 mmol L^{-1} KBH_4 achieve similar degradation rates of 75.1% and 76.5% respectively. However, when the concentration of KBH_4 solution increases to 100 mmol L^{-1}, the degradation rate of MO decreases sharply to 22.6%.

The photocatalytic degradation of MO is a pseudo-first-order reaction and its kinetics can be described as follows[28]:

$$\ln \frac{C_0}{C} = kt$$

Where k is the apparent reaction rate constant, and t is the irradiation time. The data of photocatalytic degradation rate (C/C_0 vs. t) of different samples in UV light and visible light were transferred as the equation above, and the constant k of different samples were listed in Table.1.

Table 1 k data of BiOCl and Bi/BiOCl nanosheets illuminated under UV and visible light

	BiOCl	Bi/BiOCl-5	Bi/BiOCl-12.5	Bi/BiOCl-25	Bi/BiOCl-50	Bi/BiOCl-100
UV light	0.269	0.363	0.309	0.326	0.399	0.036
Visible light	0.0019	0.0034	0.0053	0.0137	0.0147	0.0020

Under UV light illumination, all the kinetic constants of Bi/BiOCl nanosheets are higher than that of BiOCl nanosheets, except for Bi/BiOCl-100, which is well coincident with the photocatalytic degradation curve in Fig.6 (ii). For all the samples, the kinetic constants under UV light are much higher than that under visible light, indicating much better photocatalytic performance under UV light. The kinetic constant of BiOCl under visible light (0.0019) is only 7.06% of that under UV light (0.269). Bi nanoparticles modification can enhance the reaction constant to 0.0137 and 0.0147 for Bi/BiOCl-25 and Bi/BiOCl-50 nanosheets.

3.4 Photocatalytic mechanism

In a word, Bi nanoparticles modified on BiOCl nanosheets enhance photocatalytic performances under both UV and visible light irradiation, except for the Bi/BiOCl-100 nanosheets.

The mechanism of the photocatalytic activity under UV light and visible light should be discussed from the photocatalytic processes, including optical absorption, generation of photoinduced electrons and holes, transfer of the photogenerated chargers and the surface reactions of photogenerated electrons and holes, as shown in the schematic diagram of Fig.7.

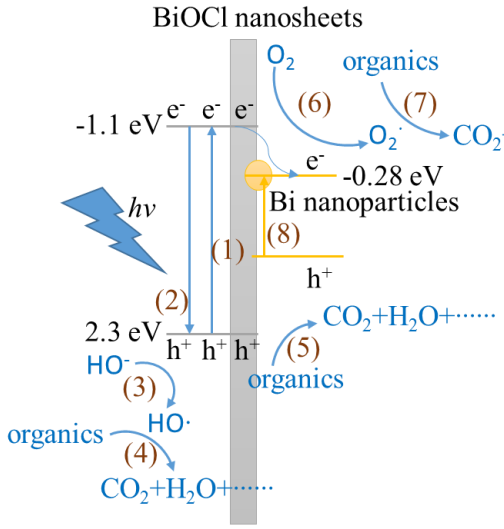

$$BiOCl + h\nu\ (UV) \rightarrow BiOCl\,(e^- + h^+) \quad (1)$$

$$e^- + h^+ \rightarrow h\nu'\ (\text{recombination}) \quad (2)$$

$$h^+ + OH^- \rightarrow HO\cdot \quad (3)$$

$$HO\cdot + \text{organics} \rightarrow \text{intermediates} \rightarrow CO_2 + H_2O + \cdots\cdots \quad (4)$$

$$h^+ + \text{organics} \rightarrow \text{intermediates} \rightarrow CO_2 + H_2O + \cdots\cdots \quad (5)$$

$$e^- + O_2 \rightarrow O_2^{\cdot-} \quad (6)$$

$$O_2^{\cdot-} + \text{organics} \rightarrow \text{intermediates} \rightarrow CO_2 + H_2O + \cdots\cdots \quad (7)$$

$$Bi + h\nu\ (Visible) \rightarrow Bi\,(e^- + h^+) \quad (8)$$

Fig.7 Schematic diagram of photocatalytic processes of BiOCl and Bi/BiOCl nanosheets

The photocatalytic processes of BiOCl nanosheets can be described as follows: When BiOCl nanosheets are excited by UV light with the energy higher than the band gap, the transition of electrons from valence band to conduction band of BiOCl forms photogenerated electron-hole pairs (as reaction (1)). Photogenerated electrons and holes will transfer to the surface of BiOCl, and part of them will recombine by emitting photons in this process (as reaction (2)). The holes can react with OH^- ions on BiOCl surface and form strong oxidizing hydroxyl radical HO· (as reaction (3)). The HO· is efficacious to degrade organic compounds into CO_2, H_2O and other inorganic substances (as reaction (4)). Also, the holes can degrade organic compounds directly (as reaction (5)) when they are captured by the organic compound on BiOCl surface. The combination of electrons and dissolved O_2 in solution produces the superoxide radicals $\cdot O_2^-$ (as reaction (6)) which are also active in organics degradation (as reaction (7)).

The visible light photocatalytic activity of Bi/BiOCl nanosheets can be ascribed to the indirect band gap transition of Bi nanoparticles on BiOCl substrate, which has been reported for photocatalytic reduction of heavy metal ions under visible light [29]. When Bi nanoparticles are excited by visible light, the indirect transition of Bi forms photogenerated electron-hole pairs (as reaction (8)). The photocatalytic degradation of organics by the photogenerated electrons and holes are same with the reaction (3), (4), (5), (6) and (7).

The generation of electron-hole pairs under illumination (reaction (1)) is the first step in the photocatalytic process and one of the key factors for photocatalytic performance of the materials. The optical absorption performances of BiOCl and Bi/BiOCl nanosheets have been discussed in Fig.5 that the Bi nanoparticles decrease the absorption in UV region and enhance the absorption in

visible region. Hence, the optical absorption is not the reason for the enhancement of photocatalytic performance.

The recombination of the photogenerated electrons and holes during charge transfer process (reaction (2)) is one of the key factors restricting the photocatalytic performance. Coupling with noble metal nanoparticles[30, 31] is an effective method to restrain the recombination of electrons and holes by transferring the electrons from conduction band of BiOCl to the nanoparticles. Compared with the metal nanoparticles deposited on BiOCl nanosheets, in situ modification of Bi nanoparticles has more advantages, such as high lattice matching in the interface, no agglomeration of nanoparticles and size controllability. The electron band of Bi nanoparticles is at -0.28 eV (vs. NHE) calculated with the work function of metallic bismuth (4.22 eV), which is more positive than the conduction band of BiOCl (-1.1 eV). When coupling well dispersed Bi nanoparticles with BiOCl nanosheets, the space charge layer at Bi-BiOCl junctions accelerates the transfer of photogenerated electrons from BiOCl to Bi nanoparticles. The separation of photogenerated electrons and holes decreases the recombination rate and enhances the photocatalytic performance.

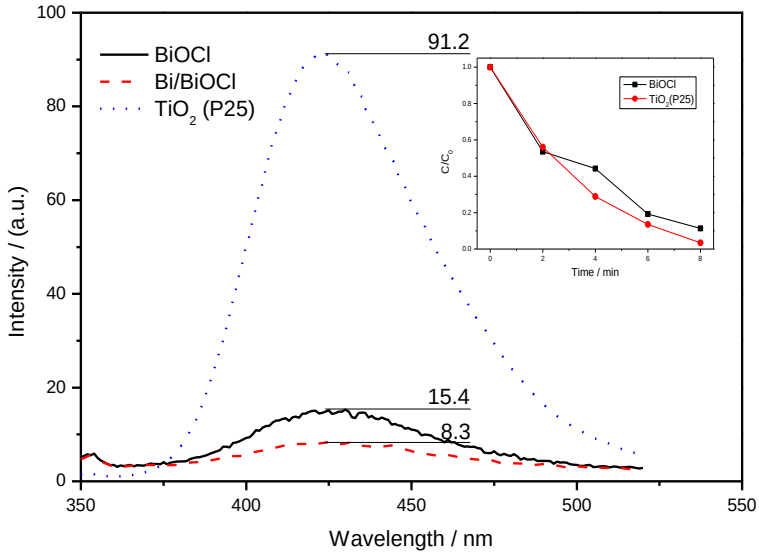

Fig.8 Photoluminescence patterns of terephthalic acid after being illuminated under UV light with BiOCl, Bi/BiOCl-25 nanosheets and TiO_2 (P25) nanoparticles, irradiation time of 15 min, inset is the comparison of photocatalytic performance between BiOCl nanosheets and TiO_2 (P25) nanoparticles

In most cases, the hydroxyl radical (HO·), holes (h^+) and superoxide radicals ($\cdot O_2^-$) are the active species in photocatalytic process. The superoxide radicals are produced by the combination of electrons and dissolved O_2. Modification of Bi nanoparticles can increase the amount of superoxide radicals in the following two aspects: the separation effects enhancing the amount of electrons and the space charge layer at Bi-BiOCl junctions accelerating the electrons to the surface.

The photocatalytic oxidation of organics by HO· and h^+ corresponds to the indirect and direct oxidations which coexist in most photocatalysts. The main oxidizing manner can be confirmed by measuring the concentration of HO· during photocatalytic process. Concentrations of HO· during photocatalytic process of BiOCl and Bi/BiOCl nanosheets were determined by terephthalic acid oxidation method. The emission intensities of dihydroxyterephthalic acid reflect the HO· concentrations. The photoluminescence patterns of terephthalic acid solution after being illuminated under UV light for 15 min with BiOCl and Bi/BiOCl-25 nanosheets are shown in Fig.8, and TiO_2 (P25) nanoparticles are used for comparison.

BiOCl nanosheets possess similar photocatalytic performance with TiO_2 (P25) nanoparticles, as shown in the inset of Fig.8. However, the HO· concentration of BiOCl nanosheets is much lower than that of TiO_2 nanoparticles, indicating that HO· is not the main active species during the photocatalytic process of BiOCl nanosheets. The direct oxidation of organics by h^+ is the main oxidizing manner. The HO· concentration of Bi/BiOCl-25 nanosheets is lower than that of BiOCl nanosheets, which may be ascribed to the consumption of HO· by electrons on well dispersed Bi nanoparticles. However it won't affect the photocatalytic performance, because HO· is not the dominating active species during the photocatalytic process.

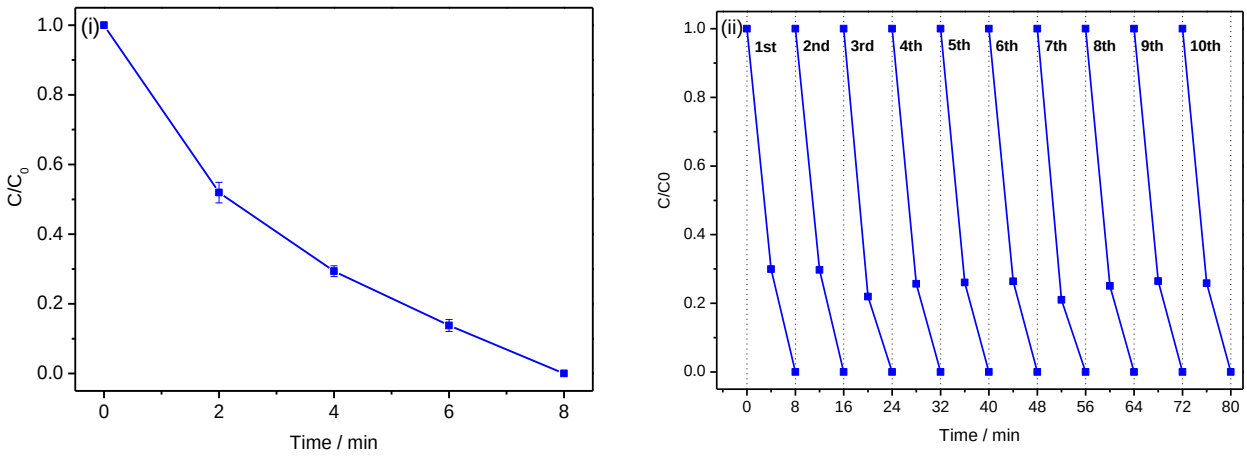

Fig.9 Technical repeatability, recyclability and chemical stability test of Bi/BiOCl-25 nanosheets under UV light illumination, (i) average degradation curve with error bar of five Bi/BiOCl-25 samples synthesized under the same condition; (ii) degradation curves of Bi/BiOCl-25 nanosheets when reused for 10 times.

Bi nanoparticles can enhance the photocatalytic performance of BiOCl nanosheets under UV light illumination via controlling photogenerated electron transfer. However, the technical repeatability, recyclability and chemical stability of Bi/BiOCl nanosheets should be considered, especially in the

UV light photocatalytic process.

Fig.9 shows the technical repeatability, recyclability and chemical stability test of Bi/BiOCl-25 nanosheets under UV light illumination. Fig.9 (i) shows the average degradation curve with error bar of five Bi/BiOCl-25 samples synthesized under the same condition, which can reflect the repeatability of the synthesis process. All the five samples can degrade the MO solution in 8 min, and the maximum error of degradation rate in 2 min is 5.6%. Fig.9 (ii) shows the degradation curves when the photocatalysts were reused for 10 times. The MO solution (20 mg mL^{-1}) can be degraded completely by Bi/BiOCl nanosheets in 8 min. The photocatalytic process was repeated for 10 times, and the photocatalyst can keep the same degradation rate, indicating the excellent recyclability of Bi/BiOCl nanosheet under UV light illumination.

The electrons transfer from BiOCl to Bi during the photocatalytic process results in high resistance to oxidation of Bi nanoparticles, which is why Bi/BiOCl nanosheets possess high chemical stability and excellent recyclability.

4 Conclusions

Bi nanoparticles modified BiOCl nanosheets were achieved via an in situ chemical reduction method in KBH_4 aqueous solution. The nanoparticles are well dispersed on the surface of BiOCl nanosheets with size of approximately 5~20 nm. And the amount of Bi nanoparticles on BiOCl nanosheets can be controlled by changing the concentration of KBH_4 solution. Bi nanoparticles can enhance the photocatalytic performance of BiOCl nanosheets in the UV region due to the separation effect of photogenerated electrons and holes. Also, Bi/BiOCl nanosheets show good photocatalytic performance in the visible light irradiation due to the indirect band gap transition of Bi nanoparticles on BiOCl substrate. When the KBH_4 concentration is around 25 mmol L^{-1}, Bi/BiOCl nanosheets achieve the best photocatalytic performance with MO degradation rate of 95% in 8 min under UV irradiation and 75% in 2 h under visible light illumination.

Acknowledgements

This work was supported by Nature Science Foundation of China (51102071, 51172059 and 51272063), Fundamental Research Funds for the Central Universities (2013HGQC0005), Nature Science Foundation of Anhui Province (1408085QE86), Anhui International Cooperation Project (1303063014).

References

[1] R. Asahi, T. Morikawa, T. Ohwaki, K. Aoki and Y. Taga, *Science.*, 2001, 293, 269.

[2] A.-L. Linsebigler, G.-Q. Lu and J.-T. Yates, *Chem. Rev.*, 1995, 95, 735.

[3] H. Liang and X. Li, *J. hazard. Mater.*, 2009, 162, 1415.

[4] L. Zhang, D. Chen and X. Jiao, *J. Phys. Chem. B*, 2006, 110, 2668.

[5] A. Iwase and A. Kudo, *J. Mater. Chem.*, 2010, 20, 7536.

[6] A. Hameed, V. Gombac, T. Montini, M. Graziani and P. Fornasiero, *Chem. Phys. Lett.*, 2009, 472, 212.

[7] H. Abdul, M. Tiziano, G. Valentina and F. Paolo, *J. Am. Chem. Soc.*, 2008, 130, 9658.

[8] H. Fu, C. Pan, W. Yao and Y. Zhu, *J. Phys. Chem. B*, 2005,109, 22432.

[9] S.-F. Chen, W.-M. Tang, Y.-F. Hu and X.-L. Fu, *Cryst. Eng. Comm.*, 2013, 15, 7943.

[10] H. Peng, C.-K. Chan, S. Meister, X.-F. Zhang and Y. Cui, *Chem. Mater.*, 2008, 21, 247.

[11] K.-L. Zhang, C.-M. Liu, F.-Q. Huang, C. Zheng and W.-D. Wang, *Appl. Cata. B: Environ.*, 2006, 68, 125.

[12] C.-F. Guo, S. Cao, J. Zhang, H. Tang, S. Guo, Y. Tian and Q. Liu, *J. Am. Chem. Soc.*, 2011, 133, 8211.

[13] C. Yu, J.-C. Yu, C. Fan, H. Wen and S. Hu, *Mater. Sci. Eng*: *B*, 2010, 166, 213.

[14] W.-J. Kim, D. Pradhan, B.-K. Min and Y. Sohn, *Appl. Cata. B: Environ.*, 2014, 147, 711.

[15] W. Xiong, Q. Zhao, X. Li and D. Zhang, *Cata. Commun.*, 2011, 16, 229.

[16] L. Kong, Z. Jiang, H. H.-C. Lai, T. Xiao and P.-P. Edwards, *Prog. Nat. Sci.: Mater. Inter.* 2013, 23, 286.

[17] J.-W. Wang, X. Wang, Q. Peng and Y.-D. Li, *Inorg. Chem.*, 2004, 43, 7552.

[18] Y.-W. Wang, J.-S. Kim, G.-H. Kim and K.-S. Kim, *Appl. Phys. Lett.*, 2006, 88, 143106.

[19] J. Toudert, R. Serna and M. Jiménez de Castro, *J. Phys. Chem. C*, 2012, 116, 20530.

[20] F. Qin, R.-M. Wang, G.-F. Li, F. Tian, H.-P. Zhao and R. Chen, Catal. Commun., 2013,42, 14.

[21] S. Weng, B. Chen, L. Xie, Z. Zheng and P. Liu, *J. Mater. Chem. A*, 2013, 1, 3068.

[22] K. Ishibashi, A. Fujishima, T. Watanabe and K. Hashimodo, *Electrochem. Commun.*, 2000, 2, 207.

[23] J. Xiong, G. Cheng, G. Li, F. Qin, and R. Chen, *RSC Advances*, 2011, 1, 1542.

[24] J. Henle, P. Simon, A. Frenzel, S. Scholz, and S. Kaskel, *Chem. Mater.*, 2007, 19, 366.

[25] E.-J. Li, K. Xia, S.-F. Yin, W.-L. Dai, S.-L. Luo and C.-T. Au, *Mater. Chem. Phys.* 2011, 125, 236.

[26] X. Zhang, Z. Ai, F. Jia and L. Zhang, *J. Phys. Chem. C*, 2008, 112, 747.

[27] K.-L. Zhang, C.-M. Liu, F.-Q. Huang, C. Zheng and W.-D. Wang, *Appl. Cata. B: Environ.*, 2006, 68, 125.

[28] H. Al-Ekabi, N. Serpone, *J. Phys. Chem*. 1988, 92, 5726.

[29] J. Zhao, Q. Han, J. Zhu, X. Wu and X. Wang, *Nanoscale*, 2014, DOI: 10.1039/C4NR01660B

[30] H.-D. Bian, Y. Wang, B. Yuan, J.-W. Cui, X. Shu, Y.-C. Wu and S.-B. Adeloju, *New J. Chem*. 2013, 37, 752.

[31] C. Yu, F. Cao, G. Li, R. Wei, J.-C. Yu, R. Jin and C. Wang, *Sep. Purif. Technol.* 2013, 120, 110.

Bi nanoparticles on BiOCl nanosheets via in situ reduction enhance the UV light photocatalytic activity and achieve visible light activity.